RSC Advances

PAPER

View Article Online
View Journal | View Issue

Cite this: *RSC Adv.*, 2022, **12**, 25605

Polydopamine surface functionalization of 3D printed resin material for enhanced polystyrene adhesion towards insulation layers for 3D microelectrode arrays (3D MEAs)†

Nilab Azim,[ab] Julia Freitas Orrico,[a] Divambal Appavoo,[a] Lei Zhai[ab] and Swaminathan Rajaraman *[acde]

3D printing involves the use of photopolymerizable resins, which are toxic and typically have incompatible properties with materials such as polystyrene (PS), which present limitations for biomedical applications. We present a method to dramatically improve the poor adhesion between the PS insulative layer on 3D printed Microelectrode Array (MEA) substrates by functionalizing the resin surface with polydopamine (PDA), a mussel-inspired surface chemistry derivative. A commercial 3D printing prepolymer resin, FormLabs Clear (FLC), was printed using a digital light processing (DLP) printer and then surface functionalized with PDA by alkali-induced aqueous immersion deposition and self-polymerization. It was observed that the adhesion of the PS to FLC was improved due to the precision emanating from the DLP method and further improved after the functionalization of DLP printed substrates with PDA at 1, 12, and 24 h time intervals. The adhesion of PS was evaluated through scotch tape peel testing and instron measurements of planar substrates and incubation testing with qualitative analysis of printed culture wells. The composition and topology of the samples were studied to understand how the properties of the surface change after PDA functionalization and how this contributes to the overall improvement in PS adhesion. Furthermore, the surface energies at each PDA deposition time were calculated from contact angle studies as it related to adhesion. Finally, biocompatibility assays of the newly modified surfaces were performed using mouse cardiac cells (HL-1) to demonstrate the biocompatibility of the PDA functionalization process. PDA surface functionalization of 3D DLP printed FLC resin resulted in a dramatic improvement of thin film PS adhesion and proved to be a biocompatible solution for improving additive manufacturing processes to realize biosensors such as *in vitro* MEAs.

Received 24th June 2022
Accepted 16th August 2022

DOI: 10.1039/d2ra03911g

rsc.li/rsc-advances

Introduction

Facile and user-friendly makerspace micro/nanofabrication technologies provide an alternative to rigorous and expensive cleanroom technologies for the fabrication of biosensors and biosystems.[1] The makerspace approach utilizes benchtop technologies, such as 3D printing, for the rapid, inexpensive, and customizable realization of devices. This approach becomes particularly important in the fabrication of non-planar devices (or 3D devices) where using lithographic or cleanroom techniques becomes challenging.[2] Previously, our group demonstrated the successful development of makerspace microfabrication technologies toward a multi-functional 3D microelectrode array (MEA) biosystem.[3] However, there are limitations of 3D MEAs prototyped by 3D printing such as toxicity issues from the photopolymerizable resin and incompatible properties with subsequent materials and functionalization.

In this previous study, we were able to define an insulation layer atop 3D topography as suggested by several other researchers[4–8] by developing another makerspace microfabrication approach utilizing "pour-spin-and-cure"[9] of biocompatible polystyrene (PS) solution.[3] The PS film not only acted as an electrical insulation layer for 3D MEAs, but also provided a barrier to prevent the leeching of some of the toxic components from the 3D photopolymerized resin to the cell culture media. Although conformal and uniform depositions of

[a]*NanoScience Technology Center (NSTC), University of Central Florida, Orlando, FL, 32826, USA. E-mail: swaminathan.rajaraman@ucf.edu*

[b]*Department of Chemistry, University of Central Florida, Orlando, FL, 32826, USA*

[c]*Department of Materials Science & Engineering, University of Central Florida, Orlando, FL, 32826, USA*

[d]*Department of Electrical & Computer Engineering, University of Central Florida, Orlando, FL, 32826, USA*

[e]*Burnett School of Biomedical Sciences, University of Central Florida, Orlando, FL, 32826, USA*

† Electronic supplementary information (ESI) available. See https://doi.org/10.1039/d2ra03911g

PS were obtained for up to 2 mm in height, we faced the challenge of PS film delamination from the 3D printed resin material, especially when the devices were placed in the incubator for *in vitro* cell culture studies. Traditional surface treatment methods such as corona treatments or plasma exposures were not enough to address this adhesion issue.[10] Plasma surface treatments are oxidative in nature and increase the polar component of the otherwise low surface energy of the treated substrate. However, these surfaces are prone to aging, or undergoing post-treatment reactions due to active sites induced by plasma. Aging effects depend on the bulk material's internal property to attain thermodynamic equilibrium by restructuring processes and diffusion, as well as external factors such as adsorption or oxidation by contaminates from atmosphere, resulting in lower surface energy.[11] Therefore, the effects of plasma treatment can be lost with time.[12]

Surface energy describes the excess energy associated with the presence of a surface and is regarded fundamental to understanding adhesion which is the force required to separate two different surfaces and is determined by the molecular interactions of the two surfaces, density of the molecules, and the contact area.[13] Adhesion strength can be improved by modifying the substrate surface by grafting, or directly coating a layer of soft polymer to increase the contact area between two surfaces of interest owing to the deformation of polymers during contact and compression.[13] Additionally, increasing the surface free energy results in improved adhesion as the chemical interactions between the two surfaces increase.

Polydopamine (PDA) has been widely investigated as a "bioglue" since 2007 due to its strong adhesion ability.[14] This mussel-inspired surface chemistry is well known for its simplicity, biocompatibility, mild processing and coating conditions, and its universal and substrate-independent applications.[15–18] PDA is formed from the self-polymerization of dopamine (DA) and the structure is dependent on the pH, time, concentration, *etc.*[19] Although the details of the mechanism of polymerization and structure still remain unknown, it is certain that the initiation of polymerization is due to dissolved oxygen and an alkaline environment that triggers oxidation by deprotonation of catecholamines followed by molecular assembly.[20] PDA has the unique ability to be deposited as a conformal thin film onto any topography and on any type of organic and inorganic surfaces *via* a dip coating process.[21–23] Previously, molecular interactions between PDA and PS was investigated and found that hydrophobic, cation–π and π–π stacking interactions contributed to the adhesion between the two materials.[24] In general, primary adhesion of PDA arises from hydrogen bonding between phenolic hydroxyl group and hydrogen bonding acceptors or even formation of covalent bonds with polar polymer surfaces, whereas hydrophobic or π–π interactions play a crucial role between PDA contacts with non-polar polymers.[14]

In this study, two surface modification techniques are explored to improve the interaction of the spin-casted PS film atop of the 3D printed substrate. We first employed a 3D printing technique called digital light processing (DLP), in which a projection method exposes an entire layer of resin at once for faster prints and allows for a higher resolution print as compared to the micro-stereolithography (μSLA) printer utilized previously.[25] Both μSLA and DLP printers have the capability to print the same commercial resin, FormLabs Clear (FLC) but result in different topographies. The high-resolution from the DLP printing technique is a mechanical method to improve adhesion. Secondly, the surfaces of the printed substrates are modified with PDA as a method of introducing chemical interactions to improve adhesion. PDA is grafted to the surface of the poly methyl methacrylate (PMMA)-based FLC resin through formation of amide bonds *via* a carbodiimide crosslinker.[26] The aromatic and hydrophobic groups from the PDA modification are expected to have improved chemical interactions with PS *via* increased surface energy and noncovalent interactions. Adhesion strength of the PS atop of the surface was characterized by incubation and subsequent scotch tape peel tests, resulting in overall improved adhesion between PS and FLC substrates (denoted as FLCS moving forward) printed *via* DLP and especially after PDA surface modification. The surface morphology, chemical composition, and surface free energy of surface before and after modification were characterized. Additionally, the substrates were tested for biocompatibility using a mouse cardiomyocyte cell line (HL-1) as these substrates are intended to be utilized as potential *in vitro* interface devices such as MEAs and other biosensors for intimate contact with cells.

Materials and methods

A general schematic of the processing methods is demonstrated in Fig. 1. First, the samples with the same dimensions were printed either using μSLA or DLP 3D printer (Fig. 1A). Subsequently, the samples were surface modified with PDA at various time intervals (Fig. 1B). Finally, PS solution was spin-cast atop of the samples and then further characterized (Fig. 1C).

Printing of planar and cell culture well substrates

Solidworks, a computer aided design (CAD) software was used to design the different substrates: flat test substrates with dimensions of 12 mm × 12 mm × 1.5 mm ($L \times W \times H$) and 3D MEA culture well substrates with dimensions of 25 mm × 25 mm base and a culture well inner diameter of 10 mm, with a height of 3 mm. FormLabs Clear (FLC) liquid resin was used for 3D printing on both FormLabs Form 2 micro-stereolithography based printer with a laser wavelength of 405 nm and Asiga MAX digital light processing (DLP) based printer with an ultraviolet light emitting diode light source (UV LED) having a wavelength of 385 nm. Important printing parameters for Asiga MAX are noted here: 50 μm layer thickness; 3 seconds exposure; and a 5 seconds burn-in layer. After the print, the substrates were removed from the stage and postprocessed according to the type of printer. The FormLabs Form 2 printed substrates were rinsed with isopropanol (IPA), placed in a sonication bath for 15 minutes, removed and rinsed once more with IPA, and finally post-bake and cure steps were performed for 15 minutes at 60 °C with UV flood exposure using

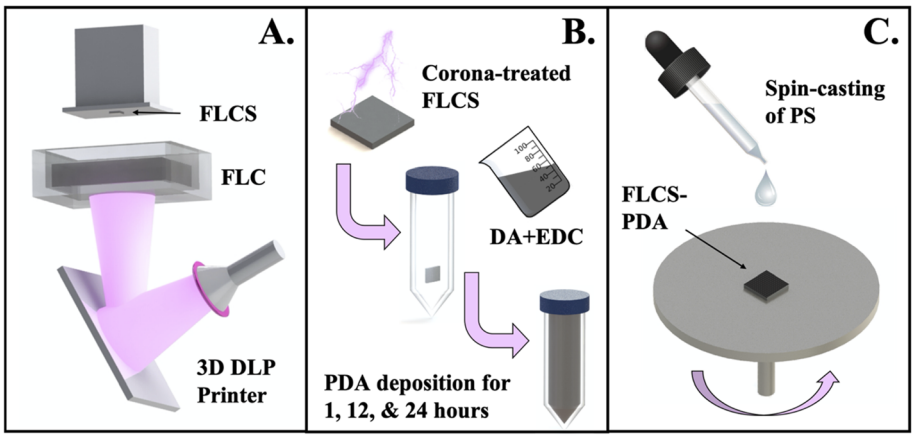

Fig. 1 General substrate processing schematic. The substrates were printed either *via* μSLA (not depicted) or DLP (depicted here) printers using FormLabs Clear liquid resin to realize FLC substrates (FLCS) (A). FLCS were then treated with corona discharge to activate the surface and then added to a solution of dopamine (DA) and crosslinker (EDC) for polydopamine (PDA) deposition times of 1, 12, and 24 hours (B). The FLCS-PDA samples were rinsed and dried and then coated with polystyrene (PS) solution using spin-casting (C).

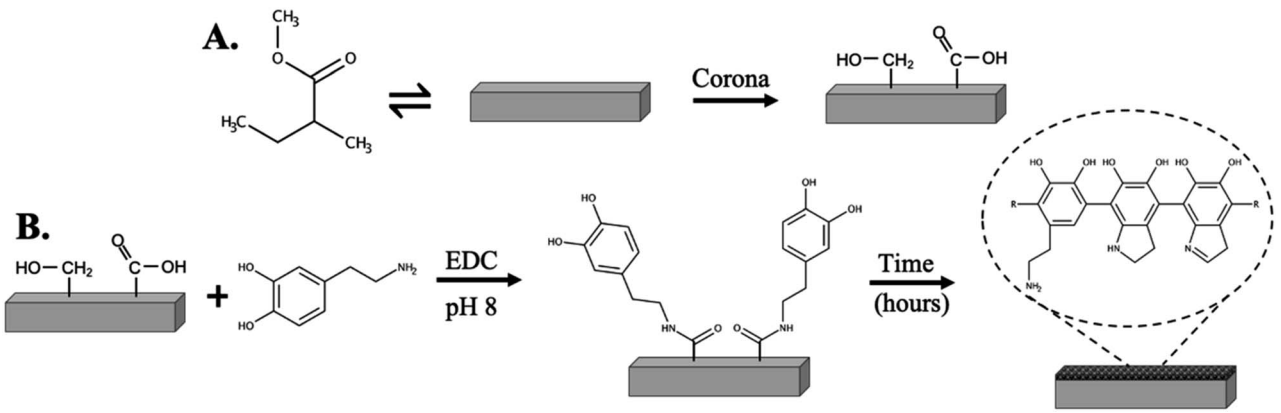

Fig. 2 Schematic of treatment of poly(methyl methacrylate)-based resin surface with corona discharge/plasma to introduce high energy functional groups (A). Schematic of potential mechanism of polydopamine conjugation and self-polymerization (B).

FormLabs Form Cure. The post-processing for the Asiga MAX printed substrates consisted of two fresh IPA baths in sonication, post-UV curing for five minutes, and a post-bake at 60 °C for 15 minutes.

Dopamine treatment

A solution of 0.05 M dopamine solution was prepared immediately before immersion of the 3D printed substrates. Deionized (DI) water was added to an appropriate weight of dopamine hydrochloride (Sigma Aldrich) in a 50 mL falcon tube and vortexed for 1 minute to dissolve. Subsequently, a two-minute ambient corona plasma (BD-20AC Laboratory Corona Treater) treated substrate was added to the solution which was magnetically stirred. Finally, an amount of 0.1 M 1-ethyl-3-(3-dimethylaminopropyl)carbodiimide (EDC) (Alfa Aesar) was added to get a 1 : 1 molar DA to EDC ratio, which resulted in an increase in pH to 8 to aid in both the conjugation of PDA onto the substrate's surface and initiation of self-polymerization. The solutions were allowed to stir in, and exposed to ambient air for either 1, 12 or 24 hours. At each respective time point, samples were removed from the PDA solution and thoroughly rinsed with DI water, three times prior to subsequent processing or characterization.

Polystyrene thin film coating

Polystyrene (PS) (~280 kDa, Sigma Aldrich) pellets were dissolved in tetrahydrofuran (THF) (Thermo Fisher Scientific) at a concentration of 20% w/v. From our previous work,[3] spin-coating (Laurell WB-400B-6NPP) parameters were optimized and found to coat films of approximate thickness, 4–5 μm at 5000 rpm for 30 seconds.[3] Therefore, these parameters were also used in this study and once PS was deposited, samples were allowed to sit at room temperature to evaporate any residual solvent. For the thermal annealing studies, samples were placed in the benchtop oven (Fisher Scientific) for 1 h at 65 °C.

Materials characterization

The FLCS composition was confirmed by Fourier transform infrared spectroscopy (FTIR) using Shimadzu IRSpirit. Due to

the thin deposition of PDA, the composition and presence was confirmed using XPS (Physical Electronics 5400 ESCA). Thickness of the deposited PDA at each time point was determined using contact mode atomic force microscopy (AFM) using Anasys Instruments NanoIR2. Topography, structure, and roughness at each time point were determined using scanning electron microscopy (SEM) (Zeiss ULTRA-55 FEG). Conditions used in the SEM include: 240× magnification; 10 kV operating voltage; 5.3–5.6 mm working distance, 5 nm Au coating and STEM detector. Images obtained from AFM and SEM measurements were analysed using Gwyddion, a data visualization and analysis software. Contact angle measurements were obtained using OCA15EC optical contact measurement apparatus by Dataphysics-Instruments. Contact angles were obtained for both water and diiodomethane and used to calculate the surface free energy change of the PDA modified surfaces at each time point using the Owens–Wendt method.[27] Mechanical testing was performed on Instron Universal tester and the samples were prepared following ASTM D638 Type I.[28] Analysis of the cross-sectioned substrates for validating the adhesion of PDA-PS to FLCS was also performed using a SEM (Zeiss ULTRA-55 FEG) and similar conditions as outlined above were used.

Biological characterization

The cell viability of the functionalized samples was tested by first attaching Asiga MAX printed FLCS to a 6-well plate with 353ND epoxy (Epotek), mixed at a 20 : 1 epoxy to cross-linker ratio. The samples were placed in an oven at 45 °C overnight, sterilized by cleaning with 70% ethanol and 24 h UV exposure using 405 nm light,[29] and finally coated with fibronectin prior to cell culturing. Approximately 330 000 HL-1 cells (a cell line derived from rat atrial cardiac myocytes) were seeded in each well of the prepared 6-well plate and cultured with supplemented Claycomb cell culture media. Cells were then maintained at 37 C in a humidified 5% carbon dioxide atmosphere. Media changes occurred every day up to five days and on the fifth day *in vitro* (DIV), a terminal live-dead assay was performed. Dead cells were stained with trypan blue (Gibco, 0.4% solution), an exclusion cell counting assay[30] to quantify the cell viability. Then, confocal imaging (Keyence BZ-X800) was performed on samples prepared by curing the FLC liquid resin within a 6-well plate and subsequent PDA functionalization and PS coating. The cell culturing protocols for imaging were the same as the cell viability tests but utilized a live/dead assay (Initrogen Live/Dead Cell Imaging Kit for mammalian cells) using a Keyence BZ-X800 All-in-One Confocal Microscope, where live cells would fluoresce green and dead cells would fluoresce red due to the uptake of calcein-AM and ethidium homodimer-1, respectively.

Results and discussions

Previously, the FormLabs Form 2 μSLA 3D printer was used to fabricate our devices and the resultant topography of the printed parts were visually observed to be rough and potentially a source of the PS adhesion issue. Thus, to study the effects of a smoother surface (*i.e.*, mechanical roughness) on adhesion, a DLP 3D printer (Asiga MAX) was employed, and the adhesion was evaluated. Next, a chemical modification with PDA was performed to improve the chemical interactions between PS and the substrate material. The PMMA-based FLCS resin structures were treated with corona, or ambient plasma, to activate the surface by introducing carboxyl and hydroxyl groups that could then react with DA in the presence of EDC to form amide bonds thereby grafting the DA to the substrate as it self-polymerizes to PDA over time (Fig. 2). The PDA was expected to have increased intermolecular interactions with PS through the hydrophobic aromatic rings, π–π bonding, and hydrogen bonding.

Mechanical and polydopamine functionalization

Planar and cell culture well substrates were printed with FormLabs Form 2 and Asiga MAX and can be observed in Fig. 3, where the Asiga MAX printed samples are qualitatively more transparent and smoother than the FormLabs Form 2 samples. The difference of topography in the two types of printers is due to the light source. FormLabs Form 2 is a laser based microstereolithographic method with a wavelength of 405 nm and a spot size of 140 μm. The diffraction of the laser as it travels through the glass and resin tank results in decreased resolution.[1] The resolution of print is also limited by the spot size and this spot-by-spot structure construction of microstereolithography printers which consequently results in a lower process throughput. However, the Asiga MAX DLP printer utilizes flashes of light from a LED source at a wavelength of 385 nm controlled by a digital micromirror device (DMD), which improves the feature sizes to a pixel resolution of 27 μm [31] which is an order of magnitude better than Form 2. Unlike μSLA, DLP allows multiple pixels on the same *XY* plane to be cured at the same time and can control the length of individual layer curing, resulting in a controlled smoother layer definition when compared to μSLA prints as observed from the prints in Fig. 3A.

Fig. 3B and C depict optical images of PDA modified planar substrates at 0, 1, 12, and 24 hours printed with FormLabs and Asiga MAX printers, respectively. There is a drastic difference in the color after modification, especially at 24 hours, which compromises the transparency of the substrate. The samples printed using Asiga MAX depict a more uniform coverage when compared to their FormLabs counterparts. However, larger aggregation coverage seemed to be concentrated in rough areas on the substrate for both sets of samples attributable to the larger surface area that PDA can deposit and hence appear concentrated in those areas.

Adhesion testing on functionalized surfaces

Previously, poor adhesion of PS films on cultures wells, printed using μSLA, was observed after incubating samples where the film would delaminate (Fig. S1A†). Culture wells provide a topographical challenge to conformal coatings of PS by providing topographical features such as sharp corners, abrupt turns *etc.* where breakage of film may occur (Fig. S1B†). This

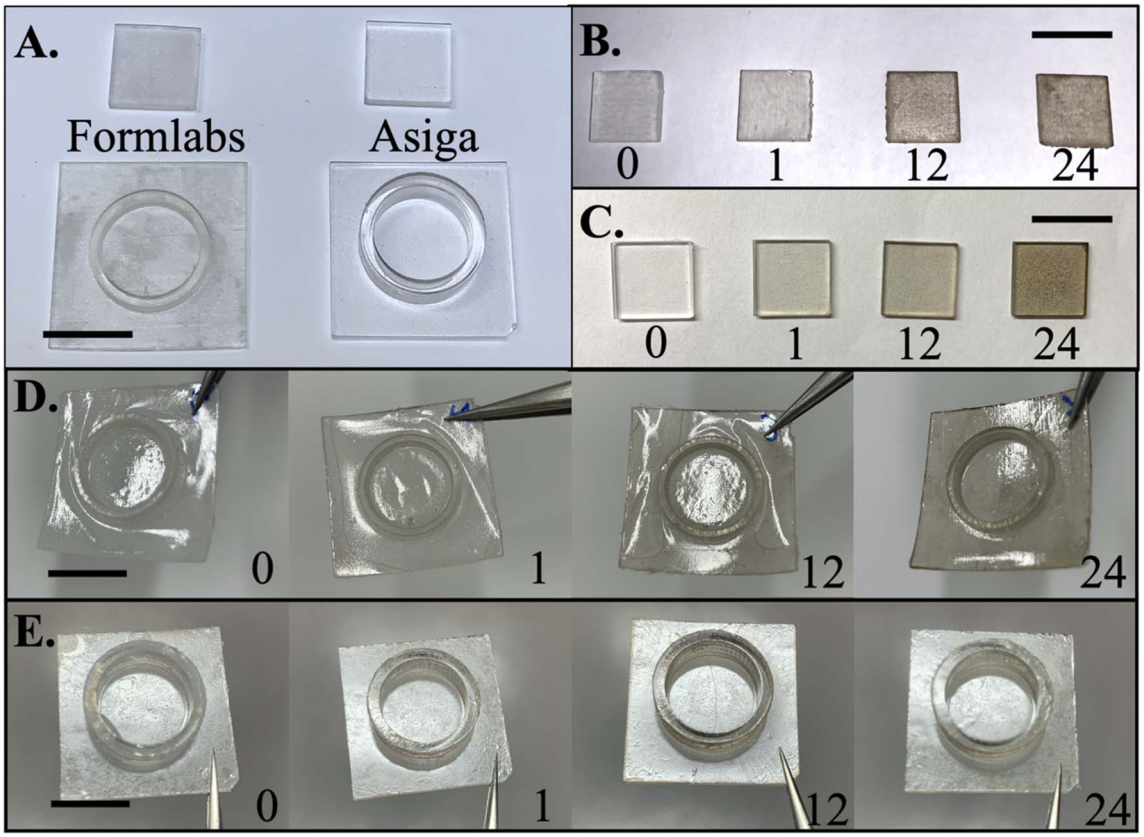

Fig. 3 Picture of FormLabs and Asiga MAX printed substrates (A) and with respective PDA modified surfaces over various periods (B) and (C). FormLabs printed culture well substrates treated with PDA at various time intervals and subsequently coated with PS after 24 hours of incubation (D). Asiga MAX printed culture well substrates treated with PDA at various time intervals and subsequently coated with PS after 24 hours of incubation (E). Scale bar is equal to 12 mm.

effect is similar to structures for 3D micro-towers in 3D MEAs as well. "Bubbling" or wrinkling of the PS was a sign of poor adhesion as solvent was able to enter and contact the underlaying substrate, simultaneously decreasing the substrate's interaction with PS. Fig. 3D provides the results of incubation tests for FormLabs printed culture wells that were treated with PDA at 1, 12, and 24 hours and then coated with PS. These samples were placed in an incubation chamber used for cells, which provided an environment that is humid and warm to test the effects on adhesion. The control, 1 and 12 hours samples resulted in bubbling, where the PS would delaminate in certain areas raising the film to look like a bubble. This was similar to what was observed in previous studies that utilized this insulation coating.[3] At 12 hours, it appeared that most of the samples had strong adhesion in the middle of the culture well and the film outside of the culture well would however delaminate. At 24 h treatment of PDA, such bubbling of the samples was not observed indicating improved adhesion in the incubator (Fig. 3D).

Interestingly for the Asiga MAX printed substrates, the adhesion after 24 h incubation was improved even without PDA modification (Fig. 3E). This is a significant discovery since most studies report the opposite to be true with smooth *versus* rough surfaces. The adhesion differences between the samples were tested briefly by utilizing a simple scotch tape peel test and this result is summarized in Table S1.† Two different parameters were tested: adhesion before and after incubation and the effect of thermal annealing on the adhesion. Thermal annealing after PS coating was performed at the glass transition temperature (T_g) of ~65 °C on the Asiga MAX samples to alleviate film formation stress and further improve adhesion. When thermally annealed, PS reaches its T_g where not only is the stress decreased on the film, but also polymer chain mobility is enhanced to improve the specific physical and chemical interactions.[32] For Asiga MAX printed samples that were not thermally annealed, especially those treated with PDA at 12 and 24 h intervals, wrinkling would be observed on samples containing 3D topographies such as culture wells (Fig. S2†) but these effects did not occur for planar samples after incubation. However, after the thermal annealing process, the wrinkling phenomenon could not be observed for any of the Asiga MAX printed samples. Thermal annealing was not performed for FormLabs printed samples as they all resulted in drastic bubbling from gas trying to escape from the grooves that were a result of the printing process, which was also a source of poor adhesion. Scotch tape peel tests (Table S1†) were only performed on Asiga MAX printed planar substates and did not demonstrate significant differences between thermally annealed samples prior to

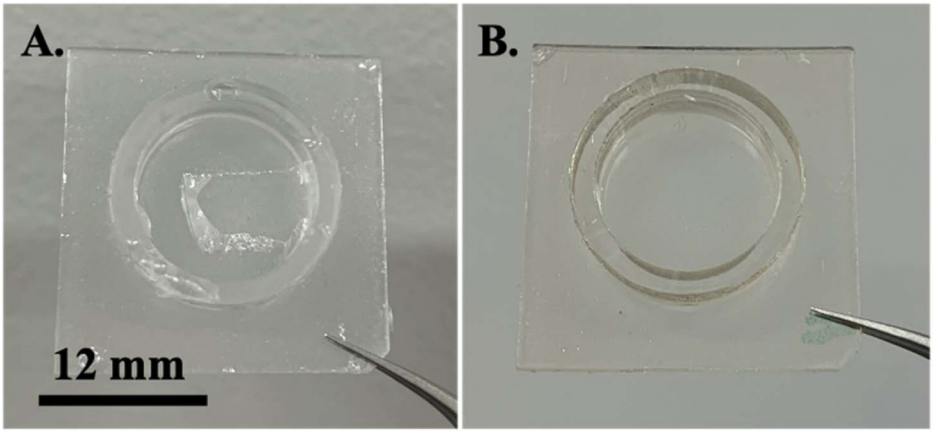

Fig. 4 Images of annealed PS film on top of control (A) and 24 h PDA treated (B) Asiga MAX printed culture wells after 24 h incubation. (A) Patch of PS film removal as result of tape peel test *vs.* (B) no PS film removal even after multiple (5×) tape peel tests.

incubation but did demonstrate a difference in adhesion after incubation. Although the control Asiga MAX printed samples did not result in bubbling, they were easily delaminated by scotch tape both before and after incubation. This indicated that thermal annealing is required for samples that contain 3D topographies such as culture wells and micro-towers (for 3D MEAs) to prevent bubbling or wrinkling when placed in an incubator. Additionally, the scotch tape peel tests confirmed that the adhesion of PS to the substrate was increased with PDA modified surfaces at each time interval but specifically, at the 24 h time period (Fig. 4).

The mechanical properties of the structures were also analysed. Dog bone shapes, following ASTM D638-Type I, were 3D printed using the DLP technique. The 3D printed structures were then spin coated with PS with/without PDA to observe any changes in the tensile strength of the material. Due to the very low PS : PMMA resin thickness ratio in the different samples, no significant difference in tensile strength was observed between the samples with/without PDA (Fig. S3A and Table S2†). Delamination of the PS in the samples without PDA was observed as the dog bone structures were being tested (Fig. S3B†). SEM analysis suggested the same result with structures without PDA demonstrating poorer adherence than structures with the PDA modification (Fig. S4†) suggesting robustness of the coatings for longer term cell culture applications.

Chemical analysis of functionalized surfaces

FTIR spectra of resins from both the printers are provided in Fig. 5A with identical profiles as expected since the same FLC resin was used for both printers. From the spectra, a signature carbonyl (C═O) is observed at 1700 cm^{-1} with an overtone at 3375 cm^{-1}, an ester (O═C–O–R) is observed at 1140 cm^{-1}, an ether (C–O–C) is observed at 1241 and 1052 cm^{-1} and methyl group (CH_3) can be seen at 2954 and 2871 cm^{-1}.[10,33] These functional moieties confirmed the resin's composition as the peaks coincided with PMMA for the most part, albeit there were two other peaks to note. Another peak at 1531 cm^{-1} that could potentially correspond to a nitrite (NO_2^-) arising from a resin stabilizer molecule. Alkene groups were also observed at 1636 and 815 cm^{-1}, indicating that there were acrylates present

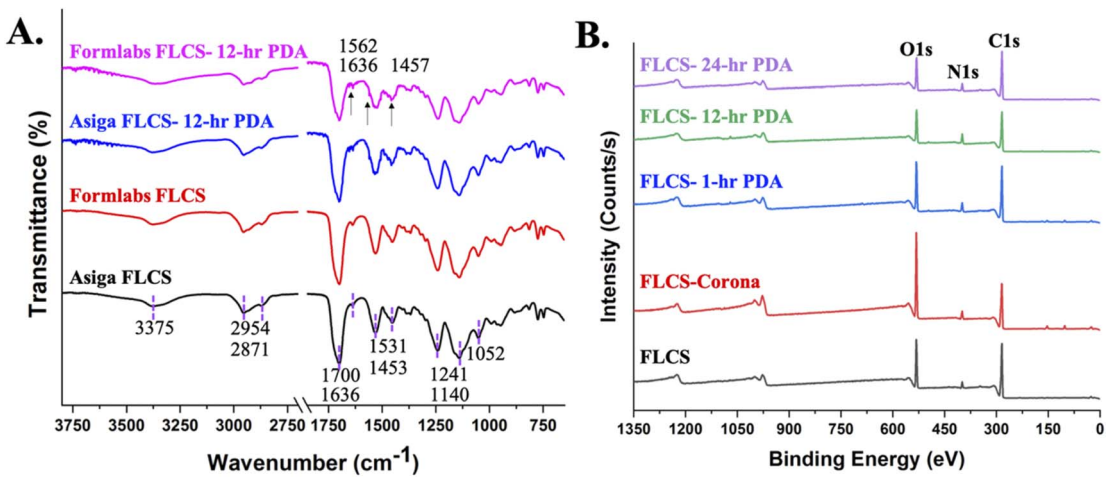

Fig. 5 FTIR (A) and XPS (B) characterization of FLCS and post PDA surface functionalization.

Table 1 XPS atomic percentages at each step of fabrication. All data reported is an average of at least $N = 3$ samples

Sample	C	O	N	N/C	N/O	O/C
FLCS	72.21	23.11	4.67	0.06	0.20	0.32
FLCS-corona	59.74	34.87	5.39	0.09	0.15	0.58
FLCS-PDA 1 h	67.86	23.92	8.22	0.12	0.34	0.35
FLCS-PDA 12 h	68.94	21.61	9.44	0.14	0.44	0.31
FLCS-PDA 24 h	68.99	21.64	9.37	0.14	0.43	0.31

possibly arising from uncured resin. However, since blanket UV post-exposure was performed as a post-processing step, this may not be likely. The FTIR spectra for 12 h PDA modified FLCS are provided as well. Although no significant peaks seem to be apparent, when looking at the fingerprint region closely, a few peaks confirm the presence of PDA deposition as indicated by the arrows in Fig. 5A. The sharp peak at 1636 cm^{-1}, newly formed peak at 1562 cm^{-1}, and sharp peak at 1457 cm^{-1} correspond to the amide C═O, N–H, and C–N moieties, respectively, bending vibrations for primary aromatic amines.[34,35]

XPS was utilized to obtain a survey spectrum of the surface and elemental regions to determine the surface atomic composition at each step and time interval (Fig. 5B). Only carbon, oxygen and nitrogen were present on all surfaces and the total atomic percentage change as a function of surface modification and this data is provided in Table 1. The corona/plasma treated samples had an expected increase in oxygen percentage from 23.11% to 34.87% as observed in the second step of surface processing but dropped back to approximately 23% after PDA treatment. Corona treatment was performed in order to activate the surface of the resin by increasing the number of carboxyl and hydroxyl groups that could potentially react with PDA. The nitrogen atomic percentage increased from 5.39% to almost 9.37% as PDA was introduced and continued to slightly increase with deposition time until 12 hours where it plateaued. The atomic ratios were calculated at each step and provided in Table 1. The ratio of N/C went from 0.065 to 0.136 and of N/O went from 0.202 to 0.433 from the unmodified surface to 24 hours of PDA deposition. The ratio of N/C was higher and of N/O was lower than the theoretical values for pure PDA (N/C = 0.125, N/O = 0.5)[36,37] though they are in the range for experimental variations from theory. As a result, we believe that these observations indicate that the surface of the FLCS is getting uniformly coated by PDA.

High resolution of XPS spectra of C 1s and N 1s were further analysed to investigate the distribution of functional groups over time to understand the mechanism of PDA modification. The peak positions and atomic concentrations of respective functional groups at each step is provided in Table 2. Although majority of the functional groups remained similar, there were some peak shifts, appearances, and intensity variations as observed in Table 2. The C 1s region was fit with six peaks assigned to C–C/C–H at ~284.8 eV, C–O at ~285.5 eV, C–OH/C–N at 286.1 eV, C═O at 288.0 eV, O–C═O at 289.1 eV, and $\pi \rightarrow \pi^*$ species.[37] The intensities of hydrophobic functional groups (C–C and C–H) decrease and hydrophilic groups (C–O and O–C═O) increase post corona surface treatment as intended to activate the surface prior to PDA functionalization.[38] The increase in C═O functional groups after PDA functionalization is attributed to intermediate quinone PDA species, indicative of degree of PDA deposition and oxidation state. Since no C–O was observed in the PDA modified surfaces, it is suggested that the C═O groups in quinones are the major oxygen functional groups. The high fraction of ester species in the FLCS and FLCS-corona treated samples, contributed from the PMMA derived commercial resin, begins to decrease with increasing PDA deposition. The small fraction of O═C–O functional groups observed in the PDA functionalized substrates may be arising from the resin underneath. However, the appearance of C 1s $\pi \rightarrow \pi^*$ shakeup for 12 and 24 h samples, which is a common energy loss feature characteristic for aromatic carbon species, suggests that increased intensity reflects increased PDA deposition. Therefore, 12 and 24 h samples are more likely to have more aromatic groups to participate in π–π stacking and hydrophobic interactions, resulting in improved adhesion.

The N 1s region was fit with four peaks assigned to tertiary/aromatic amine (R═N–R) at 398.2 eV, secondary amine (R–NH–R) at 400.0 eV, primary amine (R–NH_2) at 401.0 eV, and nitrate (R–NO_2) at 405.0 eV.[39] Secondary nitrogen species observed for FLCS confirms the FTIR measurement of nitrogen species. However, the FTIR suggested that the nitrogen containing functional group is a nitrite species, which is confirmed in the subsequent step samples, FLCS-corona, and FLCS-PDA 1 h. The corona discharge treatment most likely exposed and formed

Table 2 Summary of XPS functional group details of the various surface treated FLCS. All data reported is an average of at least $N = 3$ samples

	Peak positions, eV	FLCS	FLCS-corona	FLCS-1 h PDA	FLCS-12 h PDA	FLCS-24 h PDA
C 1s	284.8 (C–C, C–H)	45	36	54	51	43
	285.5 (C–O)	23	16	—	—	—
	286.1 (C–OH, C–N)	20	29	36	36	42
	288.0 (C═O)	—	—	1	8	9
	289.1 (O═C–O)	13	19	8	4	4
	291.5 ($\pi \rightarrow \pi^*$ shakeup)	—	—	—	2	2
N 1s	398.2 (R═N–R)	—	—	13	11	11
	400.0 (R–NH–R)	100	66	68	60	67
	401.0 (R–NH_2)	—	28	16	29	22
	405.0 (R–NO_2)	—	6	3	—	—

hydrophilic groups by etching away at the surface, which explains the introduction of the primary amine and nitrite groups. The tertiary amine peak appears for all post PDA deposition time intervals, which is associated with the intermediate tautomeric indole and quinone species of PDA. Additionally, the nitrite functional group that was associated with the FLCS resin, disappears after longer PDA deposition times (12 and 24 hours) implying that the surface begins to get completely covered and will be confirmed in subsequent testing.

Morphological analysis of functionalized surfaces

The morphology of FLCS surfaces post PDA modification printed with DLP printing were visualized by SEM and AFM as observed in Fig. 6. The SEM images indicated that PDA is deposited as dispersed accumulated nanoaggregates and with increasing coverage over time. Qualitatively, SEM images depicts increased nano-roughness with prolonged PDA deposition but at 24 hours the surface appears like a smooth film and similar to an as printed substrate (Fig. 6). The diameter and count of the aggregates are analyzed using ImageJ (NIH) software image processing tool and provided as histogram graphs in Fig. S5.† As observed from the histogram graphs with Gaussian fitting, the aggregates at 1 and 12 h deposition times are distributed similarly, with the 12 h deposition at approximately 2× counts indicating two times the coverage. The distribution of nanoaggregates at 24 hours reduces, showing a similar distribution as the control where there is no deposition of PDA, and peaks at approximately 5 nm. The 24 h PDA deposition as compared to the control substrate has almost 3× number of counts and has higher counts of larger diameter nanoaggregate materials. AFM measurements of the root mean squared (RMS) roughness is also provided for respective samples in Fig. 6. RMS roughness values indicate that 1 h deposition had the highest roughness of ~50.63 nm out of all the samples, with 12 h roughness dropping to 43.60 nm and 24 h dropping even further down from the unmodified surface to 28.68 nm. The 1 h sample roughness is most likely due to the incomplete coverage of the original surface and larger PDA nanoaggregates.

The nanoaggregates form because DA is initially grafted on the surface *via* covalent crosslinking and this material undergoes self-polymerization creating anchored polymerized PDA supramolecules which then result in physical aggregation as more PDA gets deposited. There is a competitive process of aggregation and deposition as proposed by Ding *et al.*, where DA monomers are consumed to produce either aggregates in solution or deposit on the surface. The process that prevails depends on the concentration of DA defined by the two regimes and a concentration larger than 1.0 g L^{-1} results in a dramatic reduction in the free mean path of DA monomers therefore increasing the rate of aggregation against the rate of deposition.[37] The concentrations of our solutions were ~9.5 g L^{-1}, therefore lying in regime II where aggregation is prominent, which may explain the observation of nanoaggregates for the lower time intervals at 1 and 12 hours. However, according to our results, given enough time these nanoaggregates can disappear as the concentration of PDA in solution decreases and a uniform layer of PDA can be achieved as demonstrated in the 24 h samples.

Although the size and roughness of the PDA deposition was determined, the thickness of the deposited material was still unknown. AFM was used to examine the thickness of interfaces of functionalized surfaces created by a step and scanning the profile of this region ($N = 3$). Fig. 7 shows AFM images of 1, 12, and 24 h treated PDA samples with thicknesses estimated as ~120 nm, ~60 nm, ~60 nm, respectively. Although the 1 h PDA sample resulted in a thicker deposition, it was the most inconsistent due to the large non-uniform nanoaggregate

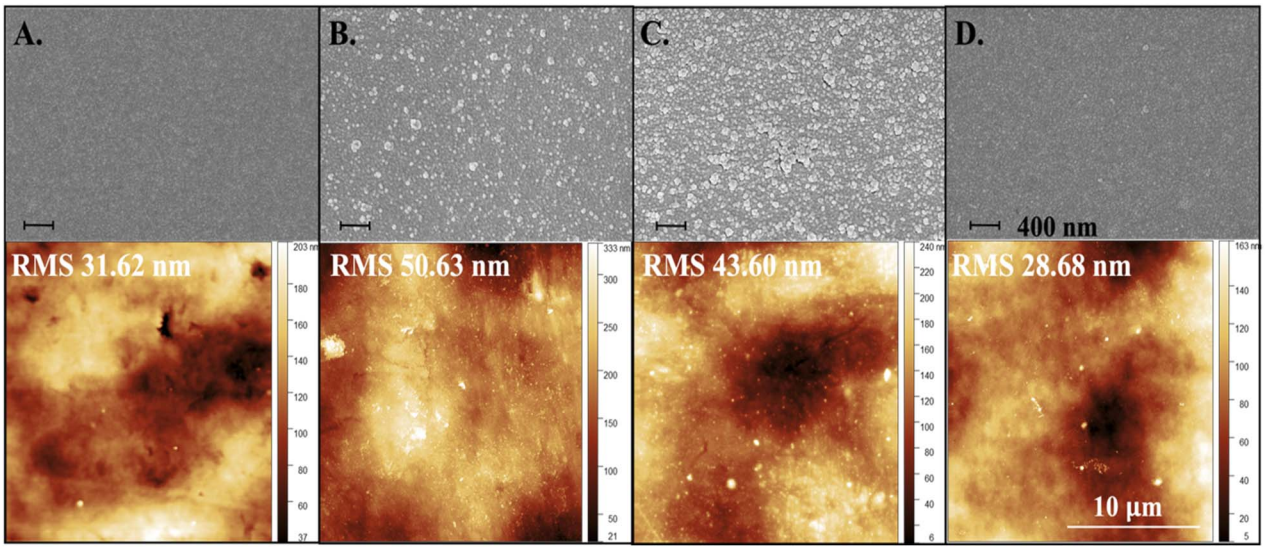

Fig. 6 SEM images of surface topography at each 0- (A), 1- (B), 12- (C), and 24-h (D) intervals with extracted PDA island aggregates and respective AFM scans with roughness measurements.

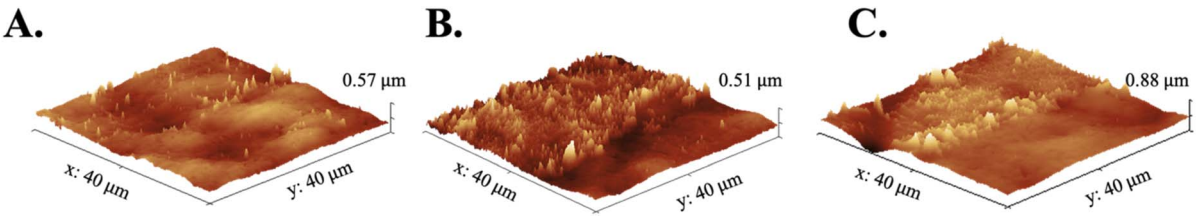

Fig. 7 Interface AFM images of FLCS coated with 1- (A), 12- (B), and 24-h (C) PDA.

Table 3 Summary of water and diiodomethane contact angles and surface free energies calculated by Owens–Wendt model of the functionalized surfaces. All data reported is an average of at least $N = 3$ samples

	Contact angles (degrees)		SFE (mJ m^{-2})		
	θ_w	θ_d	γ_s^d	γ_s^p	γ_s
FLCS	70.4	37.9	28.9	10.8	39.7
FLCS-corona	48.1	31.2	31.9	23.1	55.0
FLCS-1 h PDA	41.0	48.2	23.8	33.1	56.9
FLCS-12 h PDA	34.8	44.8	25.6	35.7	61.3
FLCS-24 h PDA	48.1	48.2	23.8	28.1	52.0

deposits as was observed in Fig. 6. The profiles of 12 and 24 h PDA treated surfaces as seen in Fig. 7B and C, respectively, further confirmed the drastic difference in topography, or roughness, resulting from the two different time intervals.

Surface free energy analysis of functionalized surfaces

It is well known that surface roughness plays a role in wettability and consequently adhesion. The extent of adhesive bonds strongly depends on the spreading ability of the deposited coating on an adherent substrate prior to drying. Wetting describes the interaction of a liquid with a solid by studying the contact angle at the solid/liquid/gas interface.[40] The wettability of samples treated with PDA was determined from water contact angles (WCA) (Fig. S6†) as summarized in Table 3. From the trend of WCA measurements, a drop is observed from ~70° to ~41° after 1 h PDA surface modification and has a unique drop to ~35° and an increase to ~48° after 12 and 24 h PDA depositions, respectively. PDA deposition increased the wettability of the substrate overall and the changes in WCA at different deposition times is most likely due to the roughness changes observed from AFM imaging. This observed decrease of WCA indicating an increase in wettability is desired as the PS solution upon deposition will result in enhanced spreading on the surface and consequently improve adhesion of the dried film.[41]

Surface free energy (SFE) provides a better understanding of the adhesion between the dried PS film and the FLCS with PDA modified surface and thus was calculated. SFE describes all the physical and chemical properties that have an influence on adhesion. Briefly, SFE is a thermodynamic quantity that describes the state of equilibrium of the atoms on the surface layer of materials reflecting the state of imbalance in intermolecular interactions present at the phase boundary of two media.[27] SFE can be calculated indirectly by the Owens–Wendt model[27] that determines the dispersive (γ_s^d) and polar (γ_s^p) SFE components separately and the sum is equivalent to the SFE (γ_s) of the surface of interest:

$$\gamma_s = \gamma_s^d + \gamma_s^p$$

The SFE components can be determined from measurements of contact angles of water (θ_w) and diiodomethane (θ_d) of the examined materials by the following equations:

$$\sqrt{\gamma_s^d} = \frac{\gamma_d(\cos\theta_d - 1) - 1 - \sqrt{\frac{\gamma_d^p}{\gamma_w^p}}\gamma_w(\cos\theta_w - 1)}{2\left(\sqrt{\gamma_d^d} - \sqrt{\gamma_d^p}\left(\frac{\gamma_w^d}{\gamma_w^p}\right)\right)}$$

$$\sqrt{\gamma_s^p} = \frac{\gamma_w(\cos\theta_w + 1) - 2\sqrt{\gamma_s^d\gamma_w^d}}{2\sqrt{\gamma_w^p}}$$

where γ_d is the SFE of the diiodomethane; $\gamma_d^p = 2.6$ mJ m^{-2} and $\gamma_d^d = 47.4$ mJ m^{-2} are the polar and dispersive components of SFE of the diiodomethane, respectively.[27] And where γ_w is the SFE of water; $\gamma_w^p = 50.8$ mJ m^{-2} and $\gamma_w^d = 22$ mJ m^{-2} are the polar and dispersive components of SFE of water, respectively.[27] Table 3 summarizes the water and diiodomethane contact angles and calculated SFE of the different surfaces. Overall, the surface functionalization with PDA resulted in a higher SFE, 52.0–61.3 mJ m^{-2}, comparable to that of just using corona treatment 55.0 mJ m^{-2}. However, unlike corona treated surfaces, PDA modified surfaces are less likely to undergo aging and provide additional chemical interactions such as π–π bonding to further improve the PS adhesion.

Biological analysis of functionalized surfaces

These modified substrates are intended to be utilized as cell culture wells and utilized as an insulation layer for 2D/3D microelectrode array biosensors for *in vitro* functional assays. Therefore, it is necessary to study if the surface coatings affect cell viability of specific functional cell lines. Cell viability on these functionalized surfaces were determined utilizing HL-1 cells, rat atrial cardiac myocytes, which are the only cardiomyocyte cell line currently available that can continuously divide, spontaneously contract, and maintain a differentiated

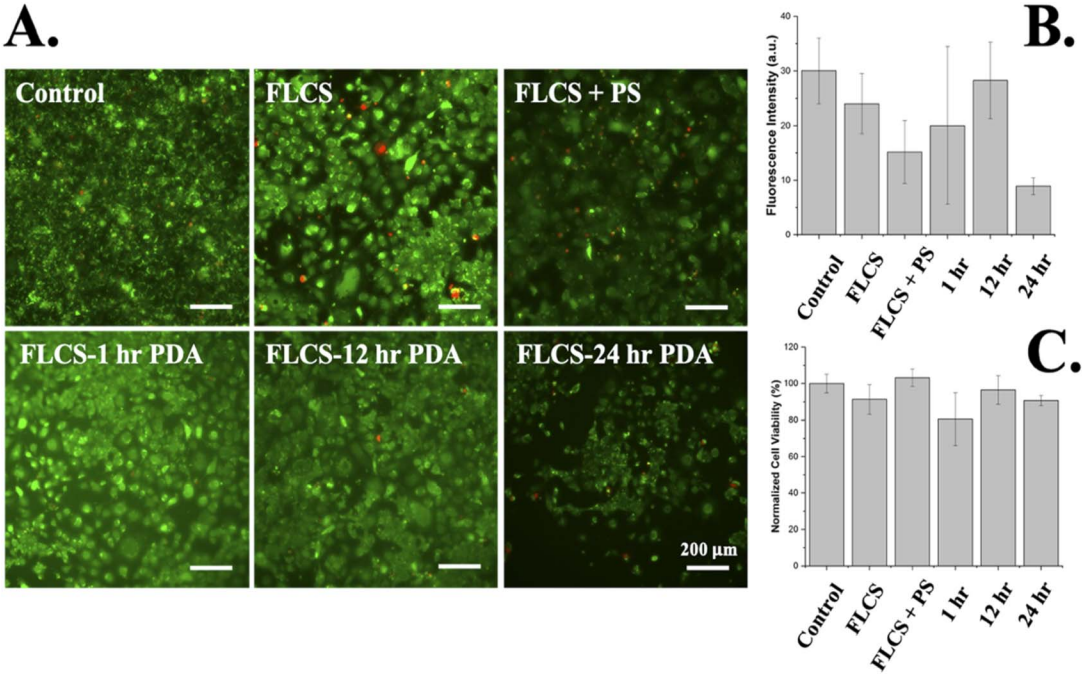

Fig. 8 *In vitro* testing of HL-1 cells by live/dead viability assay on FLCS coated with PDA and PS using confocal imaging (A), fluorescence intensity analysis of representative confocal images with the hour indicators standing for PDA treatment time (B), and cell viability by trypan blue cell exclusion assay with the hour indicators standing for PDA treatment time (C).

adult cardiac phenotype[42,43] by both live/dead fluorescence and trypan blue assays. In Fig. 8, the *in vitro* effect of the FLCS surface modifications on cell viability of the HL-1 cell line at five (5) days-*in vitro* (DIV) can be found. Fig. 8A studied the ability of confocal microscopy to image through the various layers of the substrate including FLCS, PDA, and PS. The fluorescence intensities were extracted from the confocal images and plotted in Fig. 8B to determine how much of an effect each layer had on the imaging quality. As expected, each layer contributed to a decrease in fluorescence except for samples treated with 12 h PDA, where the fluorescence was near that of the control, and decreased drastically at 24 h. The 24 h treated PDA samples drastically changed in color as observed previously in Fig. 3, which can affect cell imaging characterization as observed here. Although 12 h PDA substrates resulted in darkening of the FLCS as well, it appears that fluorescence is not affected to a great extent, making it the best potential coating time frame. The large error range for fluorescence intensity for 1 h PDA makes it difficult to draw any concrete conclusions with respect to this treatment time. Furthermore, cell viability was determined as observed in Fig. 8C, and it was concluded that all of the materials utilized as substrates were biocompatible as all the normalized viability percentages and error were above ~85%, an accepted standard for the HL-1 functional cell line.[29] Clear resin substrates in our previous study[29] reported 43.39% viability and as a result the PDA-PS treatment doubled the viability of these cells on top of 3D printed substrates. Interestingly, 1 h PDA treated samples resulted in large error ranges in viability as well suggesting that 1 h coating may not be as reproducible as 12 and 24 h PDA coated samples.

Conclusions

In this work, we have demonstrated the dramatic improvement of adhesion between PS and a commercial resin FLC by first utilizing DLP printing to improve the mechanical surface characteristics and subsequent functionalization of the surface with PDA. Both methods demonstrated improved adhesion that was tested by incubation and scotch tape peel tests. The deposition of PDA was studied in depth to understand the properties aiding in improved adhesion with PS. Characterization of PDA was performed by FTIR, XPS, SEM, AFM, CA measurements, and *in vitro* functional cell culturing. Briefly, 12 and 24 h PDA modified surfaces resulted in the best adhesions when compared to the 1 hour treated surfaces due to increased availability in aromatic rings that would participate in intermolecular bonding with the aromatic groups from PS, complete coverage of the surfaces, and high surface free energies. Although 24 h PDA surface modification resulted in the best overall adhesion of DLP printed samples, 12 h PDA may be best if utilizing fluorescence assays for confocal imaging. This work reports a biocompatible solution to improving additive manufacturing processes and adds a key technology to the ever enhancing "makerspace micro/nanofabrication" technologies toolbox. Future work will investigate the effect of PDA in aiding PS adhesion of various 3D printed topographies and the effects of PDA deposition on electrochemical properties of metallic transducing elements.

Author contributions

Nilab Azim conceived of the ideas, performed majority of the printing, coating, characterization and other experimental

work. Julia Orrico worked on the biological analysis and mechanical measurements. Divambal Appavoo performed the mechanical characterization. Nilab Azim, Prof. Lei Zhai and Prof. Swaminathan Rajaraman interpreted the results, wrote the paper, and edited it.

Conflicts of interest

Prof. Rajaraman is a co-founder and major equity holder at Primordia Biosystems that may have some interests in licensing parts of the technologies described. All other authors have no conflicts to declare.

Acknowledgements

This work has been financially supported by UCF start-up funding of Prof. Rajaraman and NIH R43ES029886. We would like to thank Kirk Scammon, Materials Characterization Facility (MCF), Advanced Materials Processing and Analysis Center, University of Central Florida (Orlando, FL, USA), for help in SEM imaging. We would also like to thank Jean Calderon and David Fox for their advice and help in chemical surface functionalization and analysis, respectively.

Notes and references

1 A. Kundu, T. Ausaf and S. Rajaraman, 3D printing, ink casting and micromachined lamination (3D PICLμM): a makerspace approach to the fabrication of biological microdevices, *Micromachines*, 2018, **9**(2), 85.

2 S. Rajaraman, S.-O. Choi, R. H. Shafer, J. D. Ross, J. Vukasinovic, Y. Choi, S. P. DeWeerth, A. Glezer and M. G. Allen, Microfabrication technologies for a coupled three-dimensional microelectrode, microfluidic array, *J. Micromech. Microeng.*, 2006, **17**(1), 163.

3 N. Azim, A. Kundu, M. Royse, Y. Y. L. Sip, M. Young, S. Santra, L. Zhai and S. Rajaraman, Fabrication and characterization of a 3D printed, microelectrodes platform with functionalized electrospun nano-scaffolds and spin coated 3D insulation towards multi-functional biosystems, *J. Microelectromech. Syst.*, 2019, **28**(4), 606–618.

4 S. Kumagai, T. Yamamoto, H. Kubo and M. Sasaki, Photoresist spray coating for 3D MEMS/NEMS, in *IEEE Nanotechnology Materials and Devices Conference (NMDC2012)*, IEEE, 2012, pp. 124–127.

5 N. P. Pham, J. N. Burghartz and P. M. Sarro, Spray coating of photoresist for pattern transfer on high topography surfaces, *J. Micromech. Microeng.*, 2005, **15**(4), 691.

6 D. S. Ginger, H. Zhang and C. A. Mirkin, The evolution of dip-pen nanolithography, *Angew. Chem., Int. Ed.*, 2004, **43**(1), 30–45.

7 M. E. Alf, A. Asatekin, M. C. Barr, S. H. Baxamusa, H. Chelawat, G. Ozaydin-Ince, C. D. Petruczok, R. Sreenivasan, W. E. Tenhaeff and N. J. Trujillo, Chemical vapor deposition of conformal, functional, and responsive polymer films, *Adv. Mater.*, 2010, **22**(18), 1993–2027.

8 A. B. Frazier and M. G. Allen, High aspect ratio electroplated microstructures using a photosensitive polyimide process, in *Proceedings IEEE Micro Electro Mechanical Systems*, IEEE, 1992, pp. 87–92.

9 T. M. Nargang, L. Brockmann, P. M. Nikolov, D. Schild, D. Helmer, N. Keller, K. Sachsenheimer, E. Wilhelm, L. Pires and M. Dirschka, Liquid polystyrene: a room-temperature photocurable soft lithography compatible pour-and-cure-type polystyrene, *Lab Chip*, 2014, **14**(15), 2698–2708.

10 V. K. Thakur, D. Vennerberg, S. A. Madbouly and M. R. Kessler, Bio-inspired green surface functionalization of PMMA for multifunctional capacitors, *RSC Adv.*, 2014, **4**(13), 6677–6684, DOI: **10.1039/C3RA46592F**.

11 D. Hegemann, H. Brunner and C. Oehr, Plasma treatment of polymers for surface and adhesion improvement, *Nucl. Instrum. Methods Phys. Res., Sect. B*, 2003, **208**, 281–286.

12 M. Modic, I. Junkar, A. Vesel and M. Mozetic, Aging of plasma treated surfaces and their effects on platelet adhesion and activation, *Surf. Coat. Technol.*, 2012, **213**, 98–104.

13 L. Gong, L. Xiang, J. Zhang, J. Chen and H. Zeng, Fundamentals and Advances in the Adhesion of Polymer Surfaces and Thin Films, *Langmuir*, 2019, **35**(48), 15914–15936, DOI: **10.1021/acs.langmuir.9b02123**.

14 H.-C. Yang, J. Luo, Y. Lv, P. Shen and Z.-K. Xu, Surface engineering of polymer membranes via mussel-inspired chemistry, *J. Membr. Sci.*, 2015, **483**, 42–59.

15 C. Schlaich, M. Li, C. Cheng, I. S. Donskyi, L. Yu, G. Song, E. Osorio, Q. Wei and R. Haag, Mussel-inspired polymer-based universal spray coating for surface modification: fast fabrication of antibacterial and superhydrophobic surface coatings, *Adv. Mater. Interfaces*, 2018, **5**(5), 1701254.

16 H. Lee, S. M. Dellatore, W. M. Miller and P. B. Messersmith, Mussel-inspired surface chemistry for multifunctional coatings, *science*, 2007, **318**(5849), 426–430.

17 J. Jiang, L. Zhu, L. Zhu, H. Zhang, B. Zhu and Y. Xu, Antifouling and antimicrobial polymer membranes based on bioinspired polydopamine and strong hydrogen-bonded poly(N-vinyl pyrrolidone), *ACS Appl. Mater. Interfaces*, 2013, **5**(24), 12895–12904.

18 R. Wang, Y. Long, T. Zhu, J. Guo, C. Cai, N. Zhao and J. Xu, Fabrication of oriented wrinkles on polydopamine/polystyrene bilayer films, *J. Colloid Interface Sci.*, 2017, **498**, 123–127.

19 C. Cheng, S. Li, W. Zhao, Q. Wei, S. Nie, S. Sun and C. Zhao, The hydrodynamic permeability and surface property of polyethersulfone ultrafiltration membranes with mussel-inspired polydopamine coatings, *J. Membr. Sci.*, 2012, **417**, 228–236.

20 J. Hong, S. Choi, D. G. Jwa, M. Kim and S. M. Kang, Mussel-Inspired, One-Step Thiol Functionalization of Solid Surfaces, *Langmuir*, 2020, **36**(6), 1608–1614.

21 J. Jiang, L. Zhu, L. Zhu, B. Zhu and Y. Xu, Surface characteristics of a self-polymerized dopamine coating

deposited on hydrophobic polymer films, *Langmuir*, 2011, **27**(23), 14180–14187.

22 Z.-Y. Xi, Y.-Y. Xu, L.-P. Zhu, Y. Wang and B.-K. Zhu, A facile method of surface modification for hydrophobic polymer membranes based on the adhesive behavior of poly(DOPA) and poly(dopamine), *J. Membr. Sci.*, 2009, **327**(1–2), 244–253.

23 J. Hyun Ryu, P. Messersmith and H. Lee, Polydopamine Surface Chemistry: A Decade of Discovery, *ACS Appl. Mater. Interfaces*, 2018, **10**, 7523–7540.

24 Q. Lu, E. Danner, J. H. Waite, J. N. Israelachvili, H. Zeng and D. S. Hwang, Adhesion of mussel foot proteins to different substrate surfaces, *J. R. Soc., Interface*, 2013, **10**(79), 20120759.

25 H. Kadry, S. Wadnap, C. Xu and F. Ahsan, Digital light processing (DLP) 3D-printing technology and photoreactive polymers in fabrication of modified-release tablets, *Eur. J. Pharm. Sci.*, 2019, **135**, 60–67.

26 R. Catarata, N. Azim, S. Bhattacharya and L. Zhai, Controlled drug release from polyelectrolyte–drug conjugate nanoparticles, *J. Mater. Chem. B*, 2020, **8**(14), 2887–2894.

27 A. Rudawska and E. Jacniacka, Analysis for determining surface free energy uncertainty by the Owen–Wendt method, *Int. J. Adhes. Adhes.*, 2009, **29**(4), 451–457.

28 A. Gleadall, W. Poon, J. Allum, A. Ekinci, X. Han and V. V. Silberschmidt, Interfacial fracture of 3D-printed bioresorbable polymers, *Procedia Structural Integrity*, 2018, **13**, 625–630.

29 C. Hart, C. M. Didier, F. Sommerhage and S. Rajaraman, Biocompatibility of blank, post-processed and coated 3D printed resin structures with electrogenic cells, *Biosensors*, 2020, **10**(11), 152.

30 W. Strober, Trypan blue exclusion test of cell viability, *Curr. Protoc. Immunol.*, 2001, Appendix 3, Appendix 3B, DOI: 10.1002/0471142735.ima03bs21, from NLM.

31 A. Kundu, P. Arnett, A. Bagde, N. Azim, E. Kouagou, M. Singh and S. Rajaraman, DLP 3D printed "intelligent" microneedle array (iμNA) for stimuli responsive release of drugs and its in vitro and ex vivo characterization, *J. Microelectromech. Syst.*, 2020, **29**(5), 685–691.

32 B. Zuo, M. Inutsuka, D. Kawaguchi, X. Wang and K. Tanaka, Conformational relaxation of poly(styrene-co-butadiene) chains at substrate interface in spin-coated and solvent-cast films, *Macromolecules*, 2018, **51**(6), 2180–2186.

33 A. K. Riau, D. Mondal, G. H. Yam, M. Setiawan, B. Liedberg, S. S. Venkatraman and J. S. Mehta, Surface modification of PMMA to improve adhesion to corneal substitutes in a synthetic core–skirt keratoprosthesis, *ACS Appl. Mater. Interfaces*, 2015, **7**(39), 21690–21702.

34 R. Batul, M. Bhave, P. J Mahon and A. Yu, Polydopamine nanosphere with in-situ loaded gentamicin and its antimicrobial activity, *Molecules*, 2020, **25**(9), 2090.

35 J. Wang, S. Zhou, J. Huang, G. Zhao and Y. Liu, Interfacial modification of basalt fiber filling composites with graphene oxide and polydopamine for enhanced mechanical and tribological properties, *RSC Adv.*, 2018, **8**(22), 12222–12231.

36 N. T. Tran, D. P. Flanagan, J. A. Orlicki, J. L. Lenhart, K. L. Proctor and D. B. Knorr Jr, Polydopamine and polydopamine–silane hybrid surface treatments in structural adhesive applications, *Langmuir*, 2018, **34**(4), 1274–1286.

37 Y. Ding, L.-T. Weng, M. Yang, Z. Yang, X. Lu, N. Huang and Y. Leng, Insights into the aggregation/deposition and structure of a polydopamine film, *Langmuir*, 2014, **30**(41), 12258–12269.

38 Y. Ma, X. Cao, X. Feng, Y. Ma and H. Zou, Fabrication of super-hydrophobic film from PMMA with intrinsic water contact angle below 90, *Polymer*, 2007, **48**(26), 7455–7460.

39 R. A. Zangmeister, T. A. Morris and M. J. Tarlov, Characterization of polydopamine thin films deposited at short times by autoxidation of dopamine, *Langmuir*, 2013, **29**(27), 8619–8628.

40 K. Grundke, Characterization of polymer surfaces by wetting and electrokinetic measurements–contact angle, interfacial tension, zeta potential, in *polymer surfaces and interfaces*, Springer, 2008, pp. 103–138.

41 C. Zhang, L. Gong, L. Xiang, Y. Du, W. Hu, H. Zeng and Z.-K. Xu, Deposition and Adhesion of Polydopamine on the Surfaces of Varying Wettability, *ACS Appl. Mater. Interfaces*, 2017, **9**(36), 30943–30950, DOI: 10.1021/acsami.7b09774.

42 S. M. White, P. E. Constantin and W. C. Claycomb, Cardiac physiology at the cellular level: use of cultured HL-1 cardiomyocytes for studies of cardiac muscle cell structure and function, *Am. J. Physiol.: Heart Circ. Physiol.*, 2004, **286**(3), H823–H829.

43 W. C. Claycomb, N. A. Lanson, B. S. Stallworth, D. B. Egeland, J. B. Delcarpio, A. Bahinski and N. J. Izzo, HL-1 cells: a cardiac muscle cell line that contracts and retains phenotypic characteristics of the adult cardiomyocyte, *Proc. Natl. Acad. Sci. U. S. A.*, 1998, **95**(6), 2979–2984, DOI: 10.1073/pnas.95.6.2979.